Article:
Ramadhan, AA orcid.org/0000-0002-0711-572X, Kapur, N orcid.org/0000-0003-1041-8390, Summers, JL et al. (1 more author) (2018) Numerical development of EHD cooling systems for laptop applications. Applied Thermal Engineering, 139. pp. 144-156. ISSN 1359-4311

https://doi.org/10.1016/j.applthermaleng.2018.04.119

Numerical Development of EHD Cooling Systems for Laptop Applications

Abdulmajeed A. Ramadhan[a,b,*], N. Kapur[a], J.L. Summers[a,c], H.M. Thompson[a]

[a] School of Mechanical Engineering, University of Leeds, UK.
[b] Department of Mechanical Engineering, University of Anbar, Iraq.
[c] Research Institutes of Sweden, Swedish Institute of Computer Science North, Lulea, Sweden.

Abstract

Electrohydrodynamic (EHD) air blowers are uniquely positioned to overcome the limitations of miniaturized mechanical fans in small-scale and consumer electronic devices. A novel cooling system design using optimized EHD blowers integrated with a plate-fin heat sink is presented and proposed for thin consumer electronics such as laptop applications. A three-dimensional (3D) numerical model is developed and validated to solve the coupled equations of EHD flow and conjugate heat transfer and predict the cooling performance of the integrated EHD system. For a range of heat sink heights from 6 to 12 mm, a parametric study is performed to investigate the influence of geometric parameters and operating conditions on the thermal performance of the EHD systems based on heat sink thermal resistance and the highest operating temperature. Numerical results demonstrate that the proposed EHD cooling system is able to provide effective cooling performance and maintain the temperature within the safe and typical operating range. Under a range of thermal design power (TDP) up to 30 W, trends of predicted operating temperatures show that the developed EHD cooling systems have great potential to compete with mechanical blowers in low-profile laptops with higher TDP, lower device height and reduced installation volume compared to a selected list of current standard laptops available commercially.

Keywords: Electrohydrodynamic (EHD) cooling system, Integrated EHD blowers, EHD flow cooled heat sink, Thermal management, Miniaturized electronic applications.

* Corresponding author.
School of Mechanical Engineering, University of Leeds, UK.
E-mail addresses: mnaarr@leeds.ac.uk , aar7sh@gmail.com (A.A. Ramadhan).

1. Introduction

The continued growing demand for smaller, thinner and more powerful consumer electronics and the associated increase in the generated heat are challenging the capabilities of conventional air cooling solutions to meet the required cooling performance. In thin electronic applications such as laptops, the integration of centrifugal fans with heat sinks is usually used as part of cooling system to dissipate the heat generated by the electronic components, maintain the processors within safe operating temperatures, and ensure the reliable operation of the device. However, when the thickness of the electronic device is reduced at given operating conditions, the performance of the cooling

system degrades due to the physical limitations in heat transfer capabilities created in both miniaturized centrifugal fan and compact heat sinks [1]. Indeed, reducing the heat sink height at a given applied thermal load results in a considerable drop in the thermal performance due to the reduction in the heat exchange area. Further degradation in the cooling performance is also created when the size of combined centrifugal fan is reduced.

Typically, the fan performance can be predicted using well-known fan scaling laws. However, an experimental study presented by Walsh et al. [2] showed that these laws are inaccurate, compared with experiments, to predict the magnitude of flow rates for miniaturized centrifugal fans. They found that the maximum flow rate can be achieved for fan aspect ratio, which is the ratio of the fan blade height to its diameter, between 0.07 and 0.16, but it is significantly reduced out of this range. Moreover, it was reported that the traditional fan scaling laws are not effective for predicting the flow characteristics of miniature centrifugal fans at low Reynolds number flows due to the increased viscous effects [3]. Indeed, as the fan becomes smaller and operates at lower rotational speeds, the boundary layers created on the fan rotors at low flow regime effectively block the flow through the fan, reducing the flow rate, and causing significant losses in the fan performance [4]. In addition, previous findings and analysis showed that the flow produced by a centrifugal blower, prior to entering heat sink fins, is non-uniform and does not enter the heat sink parallel to the fins, resulting in non-uniform flow rates within the fin channels and causing a rise in entrance pressure losses and, ultimately, a reduction in thermal performance [5]. These challenges has increased the need for new cooling techniques and effective compact thermal solutions that meet the thermal management requirements for small form factor electronic applications. Among other emerging air cooling technologies proposed as alternatives to rotary fans such synthetic jets and piezoelectric fans, electrohydrodynamic (EHD) air movers have great potential to overcome the limitations of miniaturized rotary fans in modern microelectronic applications [1]. A recent comprehensive review study on the EHD phenomenon and its applications concluded that EHD air pumps can be used ideally as cooling solutions in confined spaces, on-chip and small-scale microelectronics due to their unique feature of having a wide range of flexibility and scaling ability [6].

EHD airflow is a process of interactions between electric fields and air particles, resulting in air motion by a gas discharge across two electrodes without the need for moving parts. Basically, EHD flow occurs when a high voltage is applied between a highly curved corona electrode and a grounded surface (collector electrode), creating an electric field gradient in the air gap between them. When a sufficiently high electric field is created at the corona electrode, the surrounding air molecules are ionized. The resultant charged ions are then accelerated under the effect of electrostatic forces toward the collector electrode, transferring their momentum and energy to the surrounding neutral air particles via collisions and inducing air movement known as an ionic wind.

With the advantage of no moving parts, EHD air blowers have silent operation, flexible form factor, good reliability, uniform velocity profile, and significant flow rates. Another attractive feature can be offered by EHD air movers when they are integrated as part of the cooling system where the heat exchange surface acts as collector electrode, leading to more effective heat dissipation and a reduction in the installation space [7]. EHD technology can provide further unique means of generating airflows inside narrow channels, changing the traditional way of cooling heat sinks by rotary fans. In fact, the flow stream generated by rotary blowers to cool parallel plate-fins is associated with significant entrance pressure losses and is inefficiently to penetrate inside the narrow spaces of the closely positioned fins. In contrast, EHD devices can be fitted and installed between narrow fin channels and generate effective cooling airflow of uniform velocity profile, even at low velocities, offering a great possibility to integrate EHD blowers with heat sinks for improved cooling performance.

The literature shows that the use of EHD flow has been widely investigated either as air movers to maximize flow generation and improve conversion efficiency [8-11] or for forced convection heat transfer in general applications [12-14]. EHD driven airflows have also been investigated in many studies to generate secondary flows which disturb the bulk flow and modify the thermal boundary layer for heat transfer enhancements [15-18]. However, although the attention of most recent studies has focused on the use of EHD technology for thermal management applications such as localized cooling of microelectronic components [19-21], only few studies have investigated the integration of EHD blowers with heat sinks as cooling systems for electronic or LED applications.

Schlitz and Singhal [22] proposed an integrated EHD pump with less than 2.0 mm thickness for cooling heat sinks of low power chips. Using an electrode gap up to 1.5 mm and positive corona voltage, multi-stages of parallel emitter wires were stretched and placed over semi-cylindrical grooves made at the top of grounded heat sink plate-fins, so that the wires and the fins were in a cross arrangement. Results demonstrated that the optimal EHD cooling system was able to induce ionic wind with a maximum inlet velocity of 1.6 m/s and a pressure head up to 23 Pa using less than 3 kV operating voltage to cool a 20 W chip. No more information was provided relating to the thermal performance except an estimated comparison based on experimental results against a rotary-fan system, which revealed that, at a pressure drop of 7.3 Pa and a constant temperature difference of 40 K between the heat sink and the ambient, the EHD system was compatible with a laptop cooling system in terms of size, power consumption and weight, with approximately 40% reduction in each.

With the aim of developing cooling systems for fan-free high power generation applications, Huang et al. [23] presented an experimental study to enhance natural convection heat transfer using an EHD pump integrated with a heat sink. A framework of needle-arrayed electrodes was constructed over a heated and grounded plate-fin heat sink, such that the vertical electrode gap can be changed in a

range of 10–55 mm. Four arrays of corona needles were utilized with 4, 6, 18, and 60 needle electrodes (0.7 mm in diameter), and operated using positive and negative DC voltage in a range of 0–18 kV. Results revealed the heat transfer was increased by 3–5 times over free convection, and the array of 6 needle electrodes offered the best cooling performance.

Recently, an integration between a corona wind generator and a plate-fin heat sink was experimentally and numerically developed by Shin et al. [24] as a cooling system for LED applications. The experimental tests were conducted using a heat sink of 30 mm × 30 mm base area and 30 mm height with 10 plate fins. Four of these fins were extended in height by 20 mm and acted as collector electrodes. An array of three parallel corona wires was placed above and between the grounded plate-fins, so that the emitter wires were parallel to the fin channels. The optimized prototype demonstrated that the heat transfer was enhanced by 150% over natural convection, using a generated wind velocity up to 1.5 m/s.

The first practical and successful integration of an EHD air blower into a real-world electronic applications has been performed by Jewell-Larsen et al. [7], who replaced a mechanical fan in a laptop of a Thermal Design Power of 60 W by a compact wire-to-plate EHD blower. The results of real operation showed that the optimized EHD blower offers promising cooling performance with lower installation size and acoustic levels compared with the removed rotary fan. Although the authors included a coupled physics EHD simulation model, no information regarding the geometric dimensions or detailed results was disclosed in their paper.

The present work aims to explore the benefits of integrating miniature EHD blowers with low-profile plate-fin heat sinks as a cooling system for thin consumer electronic applications, and is the first, to the authors' knowledge, to develop 3D numerical model that solves the coupled equations of EHD flow and conjugate heat transfer. For a range of operating conditions, a parametric study is undertaken to evaluate the impact of design parameters on the thermal performance of compact EHD system based on thermal management considerations.

2. EHD Numerical Modelling

2.1 EHD governing equations

Electrohydrodynamic airflow induced by a positive corona discharge and the resulting heat transfer are described by the following equations. The electric field intensity ($\vec{E}$) created between the electrodes is described by Gauss's law,

$$\vec{\nabla}.\vec{E} = \frac{q}{\varepsilon_r \varepsilon_0} \tag{1}$$

where q is the space charge density (C/m^3), ε_r is the relative dielectric permittivity of air (≈ 1), and ε_0 is the permittivity of free space (= 8.854×10^{-12} C/V.m). This can be defined in terms of the electric potential, V, by

$$\vec{E} = -\vec{\nabla}V \tag{2}$$

The electric potential in the air is governed by Poisson's equation, which can be obtained by substituting (2) into (1),

$$\vec{\nabla}.\vec{E} = -\nabla^2 V = \frac{q}{\varepsilon_0} \tag{3}$$

The equation that couples the electrostatic and Navier-Stokes equations for the airflow is derived by combining the following three equations:

i. The electric current density equation,

$$\vec{J} = \mu_p \vec{E} q + \vec{U} q - D\,\vec{\nabla} q \tag{4}$$

where μ_p is the air ion mobility in the electric field (m^2/V.s), $\vec{U}$ is the velocity vector of airflow, D is the diffusivity coefficient of ions (m^2/s). The three terms on the right side of equation (4) represent the charge conduction (the ion movement due to the electric field), charge convection (transport of charges by the airflow), and charge diffusion, respectively [25].

ii. The continuity equation for the electric current,

$$\vec{\nabla}.\vec{J} = 0 \tag{5}$$

iii. The conservation of mass equation,

$$\vec{\nabla}.\vec{U} = 0 \tag{6}$$

Combining equations (4) and (5) and using the continuity equation (6) gives the charge transport equation:

$$\vec{\nabla}.\left(\mu_p \vec{E} q - D\,\vec{\nabla} q\right) + \vec{U}.\vec{\nabla} q = 0 \tag{7}$$

Since the value of the air velocity ($\vec{U}$), which represents the charge convection term in equation (7), is very small compared with the drift velocity of ions ($\mu_{\mathrm{p}}\vec{E}$) in the charge conduction term, it can be neglected [13]. The charge diffusion coefficient is included in equation (7) with a constant value although its effect on the numerical accuracy is relatively negligible [26].

The Navier-Stokes equations and continuity equation (6) describe the hydrodynamic part of the model for the steady state incompressible airflow under the effect of the electrostatic force,

$$\rho\vec{U}\,.\,\vec{\nabla}\vec{U} = -\vec{\nabla}p + \mu\nabla^2\vec{U} + q\vec{E} \tag{8}$$

where ρ is the air density (kg/m^3), p is the air pressure (Pa), μ is the air dynamic viscosity (Ns/m^2), and the term of $q\vec{E}$ represents the body or Coulomb force (N/m^3).

The equations of heat transfer due to the EHD airflow are governed by a coupled conjugate heat transfer model that describes the process of temperature variations and the rate of heat conduction through the heat sink surfaces in a balance with the heat transferred into the moving air by convection. In the energy equation of convective heat transfer, the Joule heating effect is included as a source term of heat generation, which is caused by the released energy due to the ion current passing through the air gap [13], and defined as $Q_{\mathrm{J}} = \mu_{\mathrm{p}} q E^2$. By neglecting viscous heating, the energy equation can be expressed for the air and the heat sink, respectively, as

$$\vec{\nabla}.\left(\rho\vec{U}\,c_{\mathrm{p}}\,T_{\mathrm{a}}\right) = \vec{\nabla}.\left(k_{\mathrm{a}}\,\vec{\nabla}T_{\mathrm{a}}\right) + \mu_{\mathrm{p}} q E^2 \tag{9}$$

$$\vec{\nabla}.\left(k_{\mathrm{s}}\,\vec{\nabla}T_{\mathrm{s}}\right) = 0 \tag{10}$$

where T_{a} and T_{s} are the air and solid (heat sink) temperatures (K), respectively, c_{p} is the specific heat of the air (J/kg.K), and k_{a} and k_{s} denote the thermal conductivity of the air and solid, respectively, (W/m.K). The coupled equations of the electric field (3), charge transport (7), airflow (6 and 8), and conjugate heat transfer (9 and 10) are solved using the commercial package, COMSOL Multiphysics (V5.1), a nonlinear partial differential equations solver based on the finite-element method. For the coupled laminar EHD flow and conjugate heat transfer, the convergence criteria was set to a relative tolerance of 10^{-3} and convergence was typically reached after 25 iterations using a Newton-type iterative method. The 3D modelling of EHD cooling system was solved using a high performance computing server (POLARIS) at the University of Leeds.

2.2 Validation of the numerical method

The accuracy of the numerical method developed in this paper for the 3D modelling of EHD flow induced through a 2 mm channel thickness is validated against a range of experimental and numerical data of a wire-to-plane EHD channel presented in [27]. A cross-section of the upper half of the EHD channel geometry of 100 mm width used in the validation model is shown in **Fig. 1**. Symmetry boundary conditions were applied at the horizontal plane centered between the channel walls and at one of the channel sidewalls of the 3D simulation domain. The numerical solution procedure, modelling parameters, and boundary conditions applied to the present numerical model for electrostatics, charge transport, and fluid dynamics, are adopted as described in [28] for the same channel geometry. The space charge density generation is modelled by applying Kaptsov's assumption [29] and using Peek's equation [30] at standard air conditions (the relative air density = the roughness factor of the wire surface = 1) to estimate the electric field strength created at the surface of the positive corona electrode. More details can be found in [31, 32]. A non-uniform mesh density of 693720 tetrahedral elements was generated for the upper half of the 3D simulation domain of 50 mm width with increased mesh refinement near the corona and collecting electrodes.

The 3D numerical solution results of the EHD flow model are shown in **Fig. 2**, which was generated at 1.0 W for a channel of height, length and width of 2 mm, 70 and 100 mm, respectively, showing the distributions of the electric potential, charge density, and air velocity induced through the channel. **Fig. 3** compares the produced flow rate of the present simulation against experimental data and 2D numerical results presented in [27] for a range of input powers. The trends reveal good agreement with an average deviation of 3.6% between the present predicted values and measured data, compared to the 2D simulation results, where the friction losses due to channel sidewalls are neglected. The benchmark results demonstrate the accuracy of the present numerical approach of 3D simulations performed using COMSOL Multiphysics to predict the EHD flow characteristics.

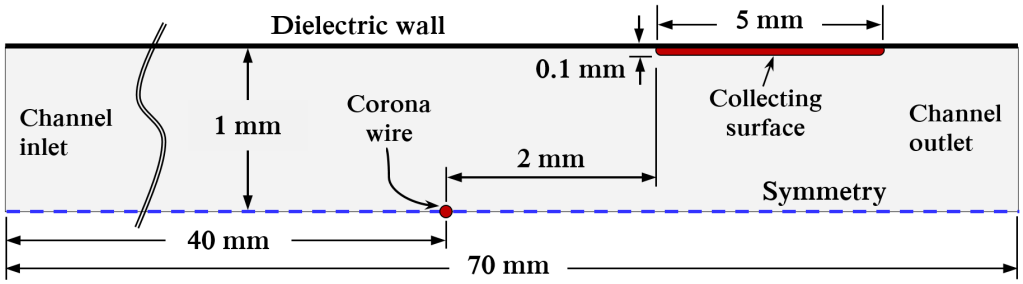

Fig. 1. Cross-section of the upper half of EHD channel geometry [27] used in the validation model.

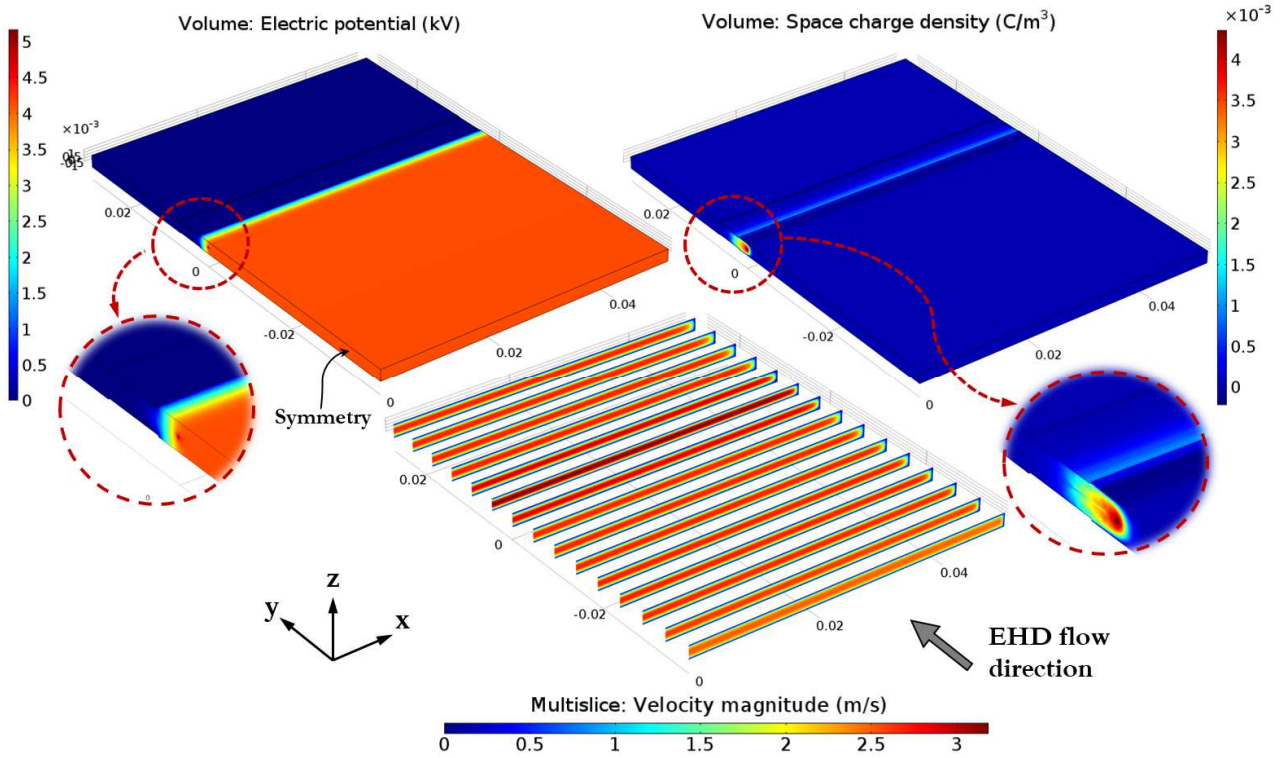

Fig. 2. Results of the 3D numerical solution of a half of EHD channel generated at 1.0 W with 2 mm thickness, 100 mm width and 70 mm length, showing the distributions of electric potential (at top-left), space charge density (at top-right), and air velocity (at bottom). Dimensions in metres.

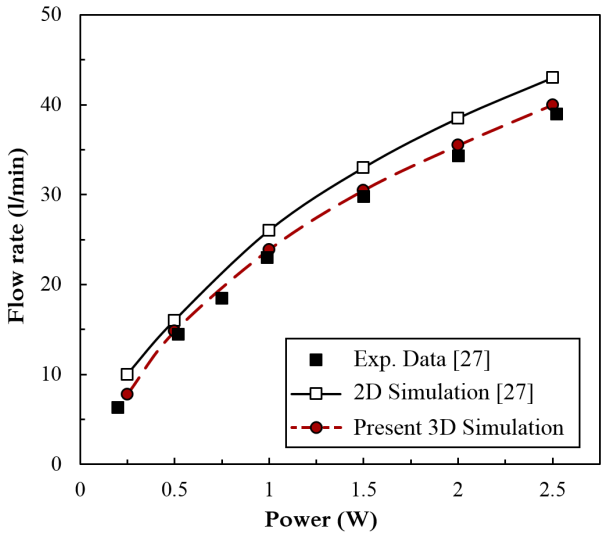

Fig. 3. Validation results of the flow rate produced by an EHD channel of height, length and width of 2 mm, 70 and 100 mm, respectively, for a range of operating powers.

3. Modelling of an EHD Cooling System

3.1 Numerical configuration

The proposed EHD cooling system mainly consists of EHD air blowers of a wire-to-plane configuration integrated with a heat sink of parallel plate fins, as shown in **Fig. 4**. Typically, plate fin heat sinks are commonly used as thermal solutions in many electronic applications such as laptops,

due to their simple design, easy manufacturing and low pressure drop, and they have lower thermal resistance compared to other types such as pin-fin heat sinks at low pumping power [33].

A simple structure of a plate-fin heat sink is employed as the heat exchange surface and acts as the collector electrode of the integrated EHD blower. The fin spacing of the heat sink is fixed at 2 mm to be within the range of channel thicknesses used in the design optimization study of miniature EHD air blowers presented in [28]. A set of fine wires of 0.025-mm-diameter are positioned vertically within the flow direction upstream of the grounded heat sink. Each wire is centered halfway between two successive collecting fins and located at a fixed distance of 1 mm from the edges of the fins and heat sink base, which is the optimal electrode gap predicted for a channel of 2 mm thickness at a constant operating power [28]. The material of the heat sink is assumed to be Aluminium with a thermal conductivity of 200 W/m.K.

In order to avoid any interference between electric fields created by corona discharge of the emitter electrodes, dielectric and insulating walls of thicknesses equal to that of the fins are used to separate the corona wires. In practical applications, these walls with a frame act as a holder of the emitter wires and also form an entrance region of the flow channels, which can be directed to the required slot in the electronic device where the cooling ambient air is pulled from. The EHD flow is induced using positive corona discharge for a range of constant operating power from 0.6 to 1.6 W, with a corresponding range of applied voltages between 3.2 and 3.7 kV. A reference model of the integrated EHD flow cooled heat sink of 10 mm height is developed to describe the modelling procedure of the coupled EHD flow and conjugate heat transfer using the geometric parameters listed in **Table 1**.

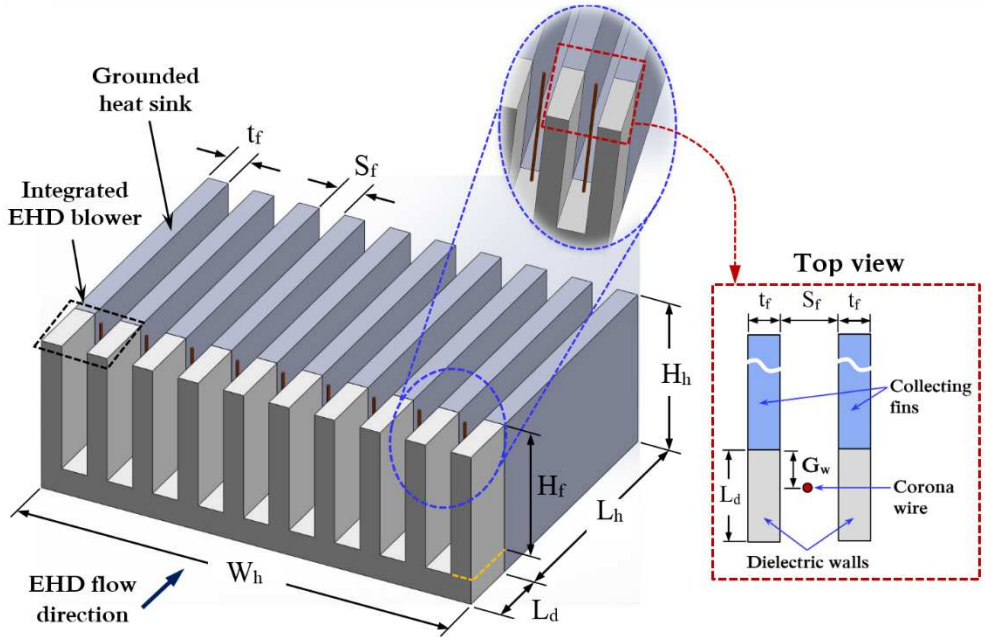

Fig. 4. Geometry of EHD cooling system, showing the integrated corona wires with a plate-fin heat sink.

Table 1. Geometric parameters and dimensions of the EHD cooling system used in the reference model.

Parameter	Value
Heat sink	
Width, W_h	70 mm
Length, L_h	30 mm
Height, H_h	10 mm
Fin height, H_f	8 mm
Fin thickness, t_f	1.6 mm
Base thickness, t_b	2 mm (= $H_h - H_f$)
Fins spacing, S_f	2 mm
Number of fins, N_f	20
Heat sink material	Aluminium (k_s = 200 W/m.K)
EHD air blower	
Electrode gap, G_w	1 mm
Number of wires, N_w	= (N_f – 1) = 19
Corona wire length	= Fin height = 8 mm
Corona wire diameter, d	0.025 mm
Dielectric walls	
Wall width	= Fin thickness = 1.6 mm
Wall length, L_d	5 mm
Wall height	= Fin height = 8 mm
Number of walls	= Number of fins = 20

3.2 Computational domain and boundary conditions

A three-dimensional computational domain of the reference model is developed for an EHD flow induced through a single fin channel to dissipate heat via convection from the surfaces of the channel base and internal walls of the two parallel fins, under a constant heat flux condition, as shown in **Fig 5**. A fine corona wire electrode is assigned vertically and centred between two parallel vertical collecting fins at an electrode gap of 1.0 mm upstream of the fin channel inlet. The length of the numerical domain is extended further at the outflow region for improved solution convergence. In order to reduce the computation time and memory, symmetry boundary conditions were applied at the vertical plane centered between the flow channel walls and at the other side of the extended region of the simulation domain. For the coupled conjugate heat transfer model, a constant heat source of 10 W is applied at the bottom surface of the heat sink base. A further heat source is applied at the corona wire due to Joule heating, while buoyancy and radiation heat transfer effects are neglected. The air temperature at the flow channel inlet is assumed to be 20 ^{o}C. The modelling parameters used in the present simulation of EHD flow are listed in **Table 2**, whereas the applied boundary conditions are summarized in **Table 3**.

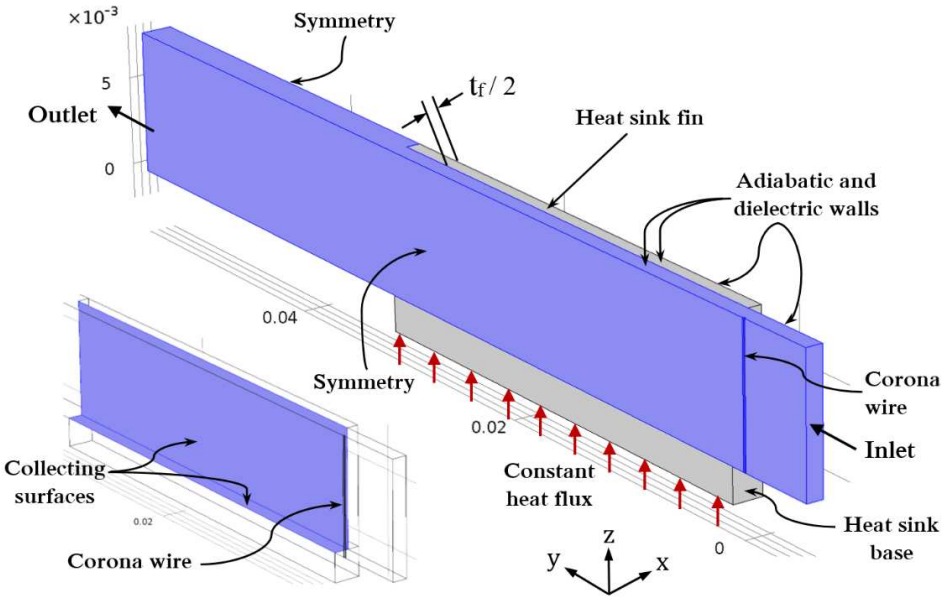

Fig. 5 Computational domain of the EHD flow and conjugate heat transfer model.

Table 2. Modelling parameters used in the EHD flow simulation of the reference model.

Parameter	**Value**
Applied potential, V_e	3.2 – 3.7 kV
Breakdown electric strength of air, E_0	3.23×10^{6} V/m
Ion mobility coefficient, μ_p	2×10^{-4} m^2/V.s
Charge diffusion coefficient, D	5.3×10^{-5} m^2/s
Density of air, ρ	1.21 kg/m^3
Dynamic viscosity of air, μ	1.82×10^{-5} N.s/m^2

Table 3. Boundary conditions applied to the computational domain for the EHD flow and conjugate heat transfer.

Boundary	**Electrostatics**	**Charge transport**	**Fluid dynamics**	**Heat transfer**
Corona wire electrode	$V = V_e$	Dirichlet condition, $q = q_0$	No-slip ($U = 0$)	$Q_J = \mu_p q E^2$
Fin surface and channel base	Grounded ($V = 0$)	Dirichlet condition, $q = 0$	No-slip ($U = 0$)	$k_a.\frac{\partial T_a}{\partial n} = k_s.\frac{\partial T_s}{\partial n}$
Dielectric channel walls	Neumann condition ($\partial V/\partial n = 0$)	Zero diffusive flux ($\partial q/\partial n = 0$)	No-slip ($U = 0$)	Adiabatic $-\vec{n}.(-k\vec{\nabla}T)) = 0$
Channel inlet	($\partial V/\partial n = 0$)	($\partial q/\partial n = 0$)	Prescribed velocity [28, 31]	$T_a = 20$ °C
Channel outlet	($\partial V/\partial n = 0$)	($\partial q/\partial n = 0$)	$P = 0$	Outflow ($\partial T/\partial x = 0$)
Air boundaries	($\partial V/\partial n = 0$)	($\partial q/\partial n = 0$)	Symmetry ($\partial U/\partial x = 0$)	($\partial T/\partial x = 0$)

A non-uniform mesh was generated for the half 3D simulation domain with increased mesh densities at the corona electrode and both heat exchange surfaces at the fin and channel base, which also act as collector electrodes, as shown in **Fig. 6**. Three mesh densities with approximately 1264390, 1449240 and 1612710 tetrahedral elements were used to solve the 3D modeling equations of EHD

flow and conjugate heat transfer. Results of mesh independency test showed that the discrepancies in the inlet average air velocity and base temperature between the second and finest densities were approximately 3% and 0.4%, respectively, as shown in **Table 4**, and therefore, the second mesh density was selected to reduce the large computational shared memory required (up to 200 GB).

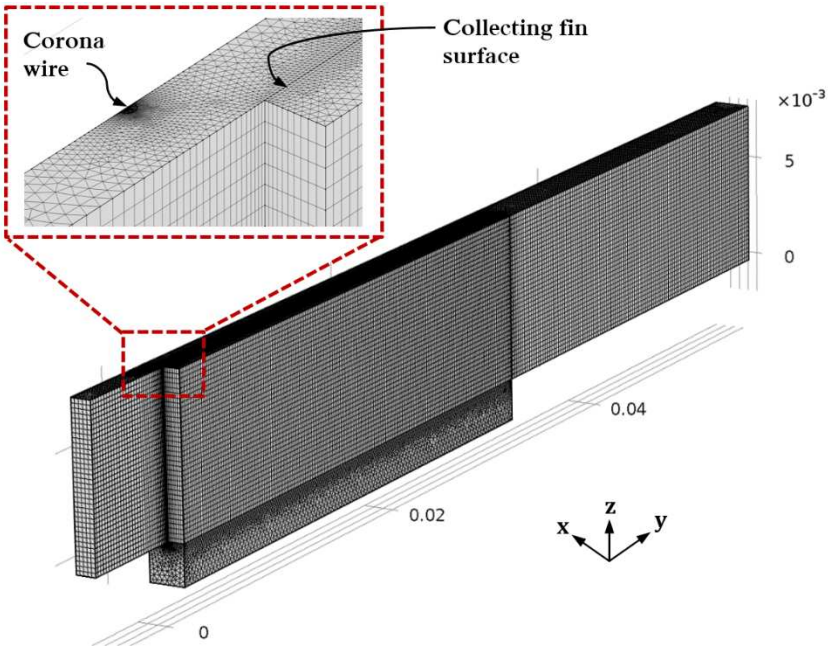

Fig. 6. Distribution of mesh element density generated for a half computational domain of fin channel with a total heat sink height of 10 mm. Dimensions in metres.

Table 4. Results of mesh independence test.

Number of mesh elements	Average velocity at channel inlet (m/s)	Discrepancy (%)	Base temperature (°C)	Discrepancy (%)
1264390	1.76	-	46.8	-
1449240	1.88	6.8	46.3	1.1
1612710	1.93	2.7	46.1	0.43

4. Numerical Results of the Reference Model

The numerical results for the integrated EHD cooling system as volume map and multislice distributions through a fins channel for electric potential, space charge density, air velocity and temperature are shown in **Fig. 7**, which are modelled at a total constant EHD power of 1.0 W and a corresponding applied voltage of approximately 3.4 kV.

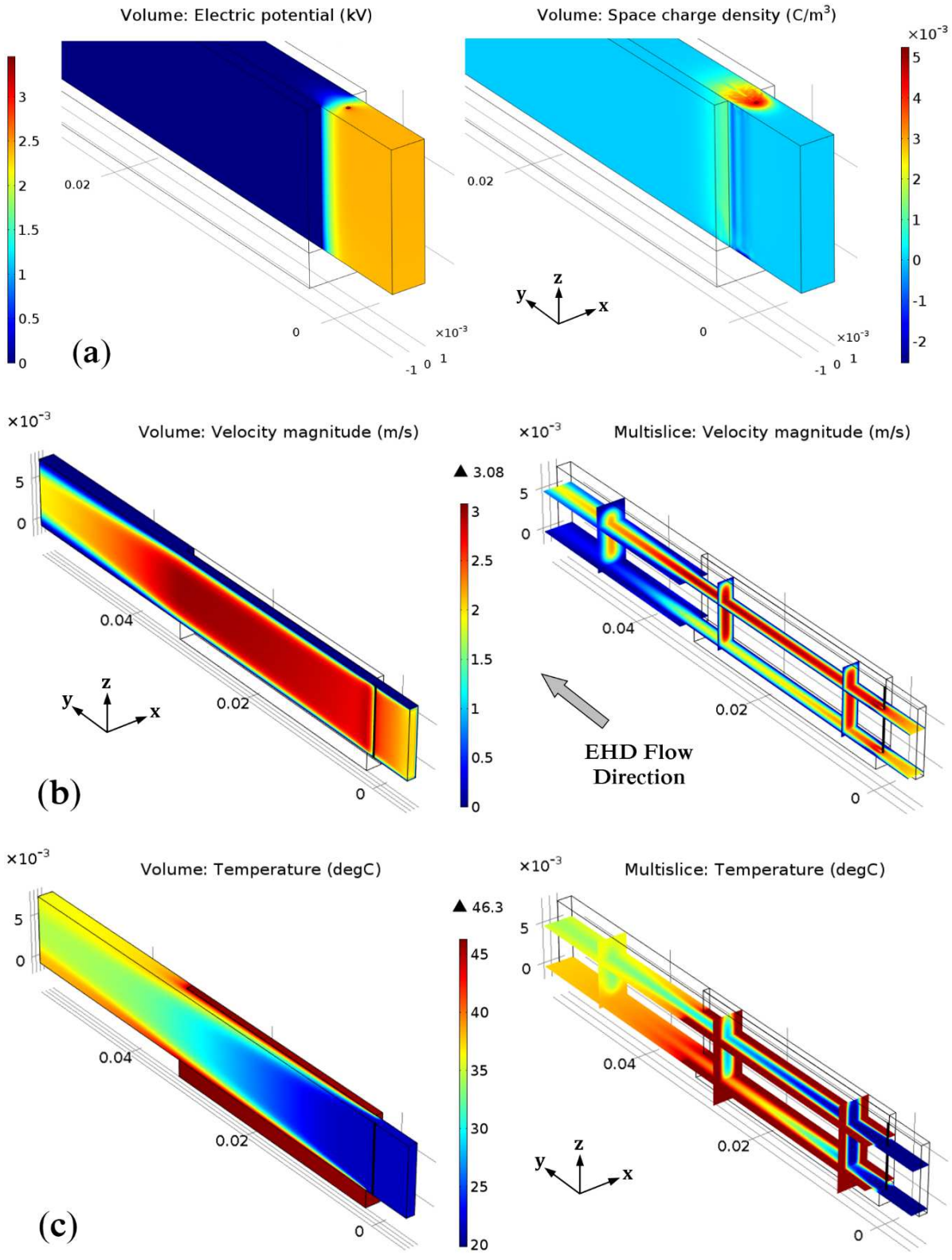

Fig. 7. Numerical solution results of the integrated EHD cooling system modelled at a constant operating power of 1.0 W for a heat sink height of 10 mm, showing the distributions of (a) electric potential and space charge density, (b) air velocity, and (c) temperature. Dimensions in metres.

The thermal performance of the developed EHD system can be characterized through the thermal resistance of the heat sink, which can be defined as,

$$R_{\mathrm{th}} = \frac{T_{\mathrm{b}} - T_{\mathrm{a}}}{Q} \tag{11}$$

where T_{b} is the highest temperature on the bottom surface of heat sink base (°C), T_{a} is the inlet air temperature (°C), and Q is heat dissipation power applied on the heat sink base (W).

Due to the absence of experimental data and numerical predictions of convective heat transfer through a channel using purely EHD driven flows in the literature, the reasonability of the present heat transfer results are verified based on a comparison with results of traditional airflow cooled heat sink under the same operating conditions and geometric dimensions. Teertstra et al. [34] presented an accurate and validated analytical model to predict the average heat transfer rate for forced convection of air cooled plate fin heat sinks. The equations of their analysis are summarized below.

The Nusselt number can be calculated from the following developed equation,

$$Nu = \left[\left(\frac{Re^* \times Pr}{2} \right)^{-3} + \left(0.664 \sqrt{Re^*}\, Pr^{(1/3)} \sqrt{1 + \frac{3.65}{\sqrt{Re^*}}} \right)^{-3} \right]^{(-1/3)} \tag{12}$$

where Pr is the Prandtl number ($= \mu c_{\mathrm{p}}/k_{\mathrm{a}}$), and Re^* is a modified channel Reynolds number, defined as,

$$Re^* = \frac{u_{\mathrm{c}}\, S_{\mathrm{f}}}{\nu} \frac{S_{\mathrm{f}}}{L_{\mathrm{f}}} \tag{13}$$

where μ is the dynamic viscosity of air (N.s/m^2), c_{p} the specific heat of air at constant pressure (J/kg.K), k_{a} is the thermal conductivity of air (W/m.K), ν is the kinematic viscosity of air (m^2/s), u_{c} is the fin channel inlet velocity (m/s), S_{f} is fin spacing (m), and L_{f} is the fin length in the flow direction (m).

The average heat transfer coefficient, h_{a} (W/m^{2}K) is given by,

$$h_{\mathrm{a}} = Nu\, \frac{k_{\mathrm{a}}}{S_{\mathrm{f}}} \tag{14}$$

The efficiency of the fins may be calculated by

$$\eta_{\mathrm{f}} = \frac{\tanh(m\,.\,H_{\mathrm{f}})}{m\,.\,H_{\mathrm{f}}} \tag{15}$$

where H_{f} is the fin height (m), and m is given by $m = \sqrt{2h_{\mathrm{a}}/k_{\mathrm{s}}\,t_{\mathrm{f}}}$, where k_{s} is the thermal conductivity of fin material (W/m.K), and t_{f} is the fin thickness (m). Thus, the thermal resistance of the heat sink is given by,

$$R_{\mathrm{hs}} = \frac{1}{h_{\mathrm{a}}\,(A_{\mathrm{b}} + \,\eta_{\mathrm{f}}\,N_{\mathrm{f}}\,A_{\mathrm{f}})} \tag{16}$$

where A_{b} is the exposed base surface area $(= (N_{\mathrm{f}} - 1)\,S_{\mathrm{f}}\,L_{\mathrm{f}})$, (m^2), A_{f} is the heat transfer area per fin $(= 2\,H_{\mathrm{f}}\,L_{\mathrm{f}})$, (m^2). However, in order to obtain the total thermal resistance, R_{th}, it is necessary to add the thermal conduction resistance across the base of the heat sink, R_{b}, which is defined as,

$$R_{\mathrm{b}} = \frac{t_{\mathrm{b}}}{k_{\mathrm{s}}\,W_{\mathrm{h}}\,L_{\mathrm{h}}} \tag{17}$$

where t_{b} is the base thickness (m), and W_{h} and L_{h} are the width and length of the heat sink (each in m). Therefore, the total thermal resistance of the heat sink can be given as,

$$R_{\mathrm{th}} = R_{\mathrm{hs}} + R_{\mathrm{b}} \tag{18}$$

Fig. 8 shows the heat sink thermal resistance obtained from the present 3D model of EHD system and that calculated from Eq. (18) as a function of the channel inlet average velocity, using the heat sink geometric dimensions presented in **Table 1**. In the EHD model, the channel velocity is averaged at the fin channel inlet plane, downstream of the corona wire. Results show that the integrated EHD system is able to provide thermal performance close to that obtained by traditional air movers at a given inlet channel velocity. However, although the mechanism of generating airflow is different, the trends reflect the capability of miniature and low profile EHD blowers to dissipate heat through narrow channels within the expected heat transfer rates with slight deviations. Indeed, the differences in the predicted results are expected as the assumptions used in the analysis reported in [34] are valid for fins with high aspect ratio ($S_{\mathrm{f}} \ll H_{\mathrm{f}}$), where the effects of the channel base is neglected.

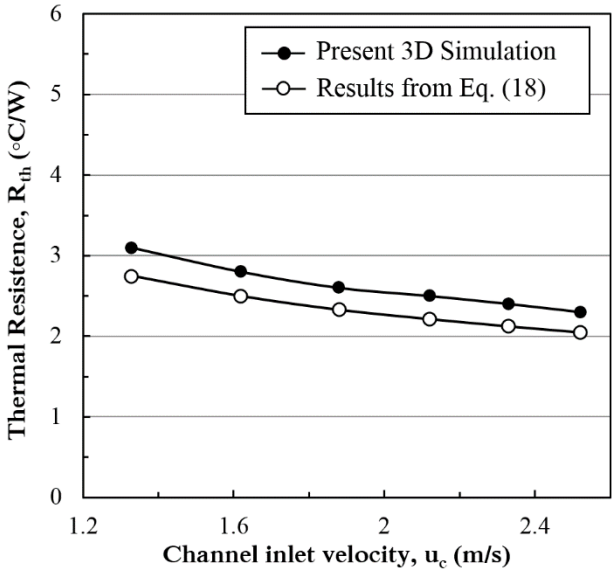

Fig. 8. Effect of the channel inlet velocity on heat sink thermal resistance for the present EHD model and that calculated analytically for traditional air cooling [34].

5. Parametric Study of the EHD Cooling System

A parametric study was performed using the developed 3D conjugate heat transfer models to evaluate the thermal performance of a plate-fin heat sink cooled by integrated EHD air blowers. The study was established to investigate the effect of the main design dimensions of heat sink structure (height, length, and width) on the heat transfer characteristics for a range of operating conditions, whereas the other geometric parameters are fixed in all investigations, as listed in **Table 5**. It is useful to mention that, at a fixed fin thickness and fin spacing, the number of fins can be used to control both the heat dissipation area (or the increased heat sink width), and the total consumed power (or the number of integrated corona wires), at a given operating power per wire.

Table 5. Fixed geometric parameters of the heat sink structure used in the parametric study.

Fixed Parameter	**Value**
Fin thickness, t_f	1.6 mm
Fin spacing, S_f	2 mm
Heat sink base thickness, t_b	2 mm (= $H_h - H_f$)
Electrode gap, G_w	1 mm
Corona wire diameter, d	0.025 mm
Corona wire length	= fin height, H_f
Number of wires, N_w	= Number of fins (N_f) – 1

5.1 Influence of heat sink height, H_h

This section studies the influence of heat sink height on the cooling performance for a heat sink length, width, and number of fins of 20 mm, 70 mm, and 20, respectively. The total heat sink height (including the base thickness) was varied from 6 to 12 mm (in 2 mm steps), which lay within the range of the thinnest ultra-thin laptops currently available (10.16 – 16.5 mm) [35]. **Fig. 9** shows the effect of heat sink height on both the thermal resistance and total operating power consumed by the integrated corona wires. The value of applied voltage is fixed at 3.4 kV to ensure generating a constant flow velocity through fin channels for all heights. The trend of total power, which is calculated by multiplying the number of wires by the power consumed by each wire, shows a linear increase as the heat sink becomes thicker due to the increase in the lengths of the corona wires at a fixed applied potential. In contrast, increasing the height extends the heat exchange area of the fins, leading to a higher heat transfer rate and lower thermal resistance at constant inlet air velocity and thermal load.

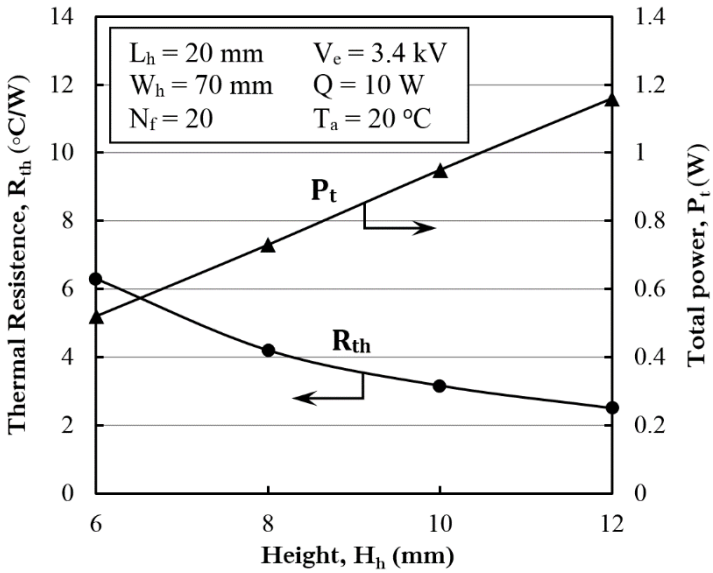

Fig. 9. Effect of heat sink height on thermal resistance and total operating power.

5.2 Influence of the number of fins, N_f

The effect of increasing the number of fins, which is associated with increasing the heat sink width, on the thermal resistance, base temperature, and power consumption is discussed here for a range of heat sink heights. The EHD blowers are operated at a fixed applied voltage of 3.4 kV for all heights and widths, generating a constant channel inlet velocity of approximately 2 m/s. **Fig. 10(a)** shows that the heat sink thermal resistance for each height decreases as the number of fins (or heat sink width) increases due to the increase in the heat dissipation area at a given thermal load, resulting in a significant drop in the base temperatures, as shown in **Fig. 10(b)**. However, the advantage of

increasing the heat transfer due to extending the heat sink width is associated with an increase in the EHD power consumption due to increasing the number of corona wires, as shown in **Fig. 10(c)**. In fact, the number and length of corona wires, and the level of applied voltage are the main factors that determine the level of power consumption of the integrated EHD blowers at a given electrode gap. The trends also can reflect a relationship between the heat sink width and power consumption based on the height parameter. For instance, in order to maintain the operating temperature at 70 ºC under a thermal load of 10 W, the EHD cooling system of H_h = 12 mm requires only 10 fins with 34 mm width, and 0.55 W of power. However, with decreasing the height of the same cooling system to 6 mm, the number of fins, heat sink width and total power are required to increase to 25, 88 mm and 0.66 W, respectively, in order to maintain the maximum operating temperature at the given level.

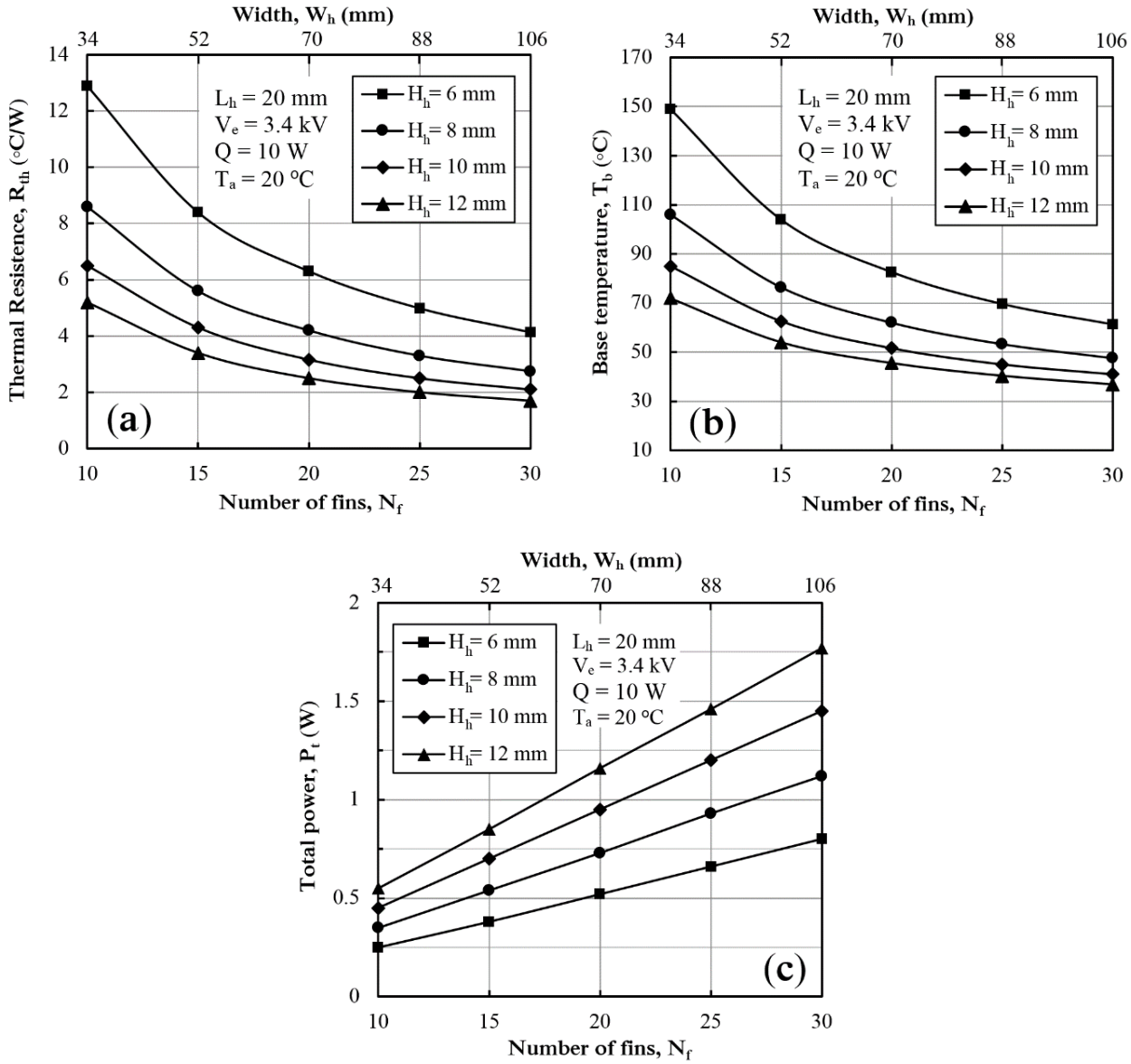

Fig. 10. Effect of the number of fins (or heat sink width) on (a) thermal resistance, (b) base temperature, and (c) total operating power, for a range of heat sink heights.

5.3 Influence of heat sink length, L_h

In this section, two heat sink heights of 6 and 10 mm with a fixed width of 70 mm are selected to study the effect of the length parameter on the thermal resistance and base temperature. The total EHD power is fixed at 0.57 W (0.03 W per wire) and 0.95 W (0.05 W per wire) for the heights of 6 and 10 mm, respectively.

Fig. 11 shows that both thermal resistance and base temperature decrease for both heights as the length of the fin channels is extended due to the associated increase in the heat dissipation area. In this case, increasing the heat sink length is independent of the operating power or the number of integrated wires. It can be seen that increasing the length from 10 mm to 50 mm, at a given operating power and fixed width, leads to a drop in the base temperature from 105 to 68 ºC and from 65 to 44 ºC, for the heights of 6 and 10 mm, respectively. However, the trends of base temperature show that increasing the length beyond 40 mm leads to a slight drop in the temperature of only 1.0 ºC for both heights. This, indeed, is attributed to the increase in the flow resistance and friction losses through the fin channels at a given induced air velocity.

Referring to the given example in the previous section, it can be seen here that the thin heat sink of H_h= 6 mm is able now to maintain the operating temperature at 70 ºC with less width (70 mm) and lower total power (0.57 W), by doubling the heat sink length from 20 to 40 mm, under the same operating conditions. It is very important that these factors are carefully taken into consideration for the efficient design of EHD cooling systems.

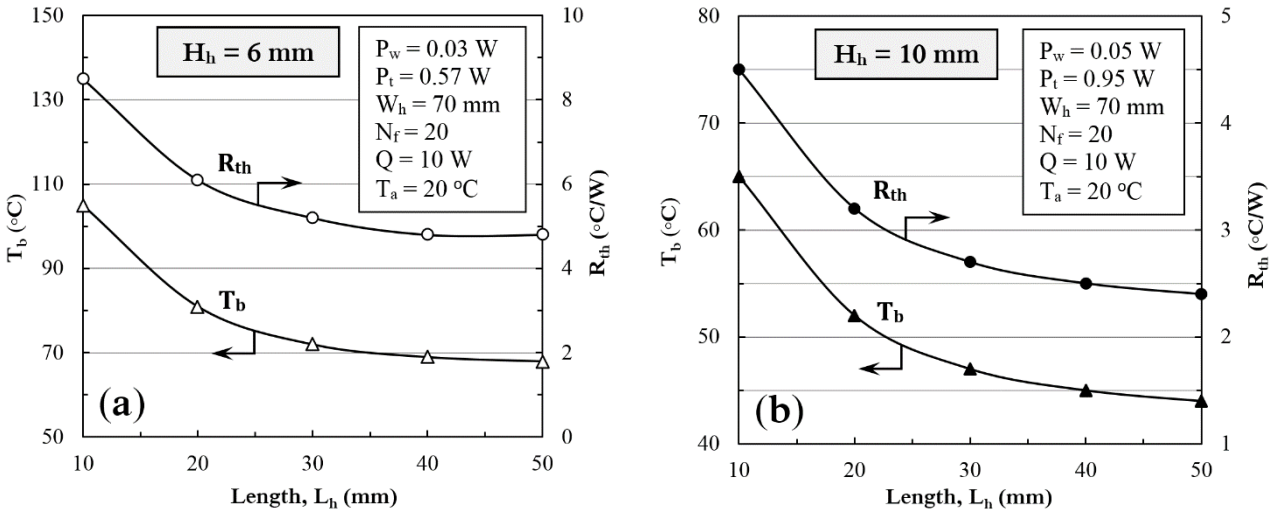

Fig. 11. Effect of heat sink length on both base temperature and thermal resistance for heights of (a) 6 mm and (b) 10 mm.

5.4 Influence of operating power, P_t

This section discusses the influence of operating power on the thermal and flow characteristics for two levels of heat sink heights (6 and 10 mm), while fixing the parameters of width and length at 70 and 30 mm, respectively. In this case, the total power and the induced air velocity increase due to increasing the level of applied potential, at a given number of corona wires.

It can be seen from **Fig. 12** that increasing the operating power from 0.3 to 0.8 W for the thinner EHD cooling system under a constant heat generation source can double the air velocity magnitude (from 1.2 to 2.3 m/s) and decrease the base temperature by 19 °C (from 86 to 67 °C) but with an increase in the required applied voltage by 0.45 kV (from 3.2 to 3.65 kV).

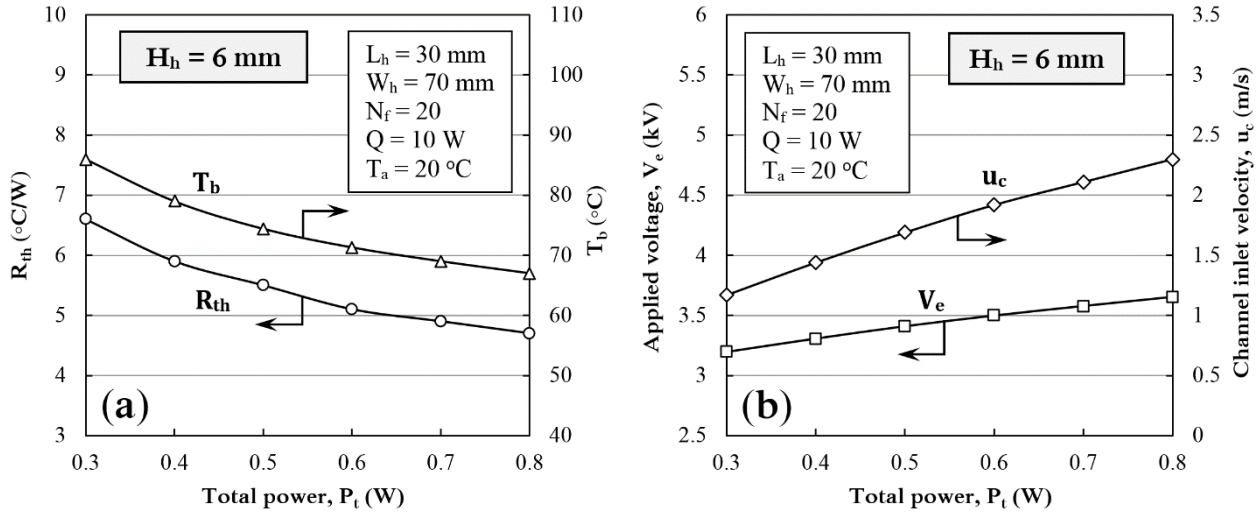

Fig. 12. Effect of operating power on (a) thermal resistance and base temperature, and (b) applied voltage and channel inlet velocity, for an EHD cooling system of H_h = 6 mm.

Similar trends with different values can be noticed for the thicker EHD cooling system of H_h= 10 mm, as shown in **Fig. 13**. The predictions reveal that increasing the total power up to 1.6 W can generate an inlet air velocity of 2.5 m/s and decrease both the base temperature and thermal resistance to 43 °C and 2.3 °C /W, respectively, using 3.7 kV operating voltage. The trends of temperatures show that increasing the total power over 0.6 W (**Fig. 12**) and 1.2 W (**Fig. 13**) for the heights of 6 and 10 mm, respectively, does not lead to a significant drop in the maximum temperature, despite the associated increase in the induced air velocity. Therefore, in the case of applying higher thermal loads or if it is required to decrease the maximum temperature further, it is recommended for both heights to increase the heat dissipation area (by increasing the number of fins) and the number of integrated wires (the total power) rather than increasing the consumed power per wire that also requires higher applied voltage.

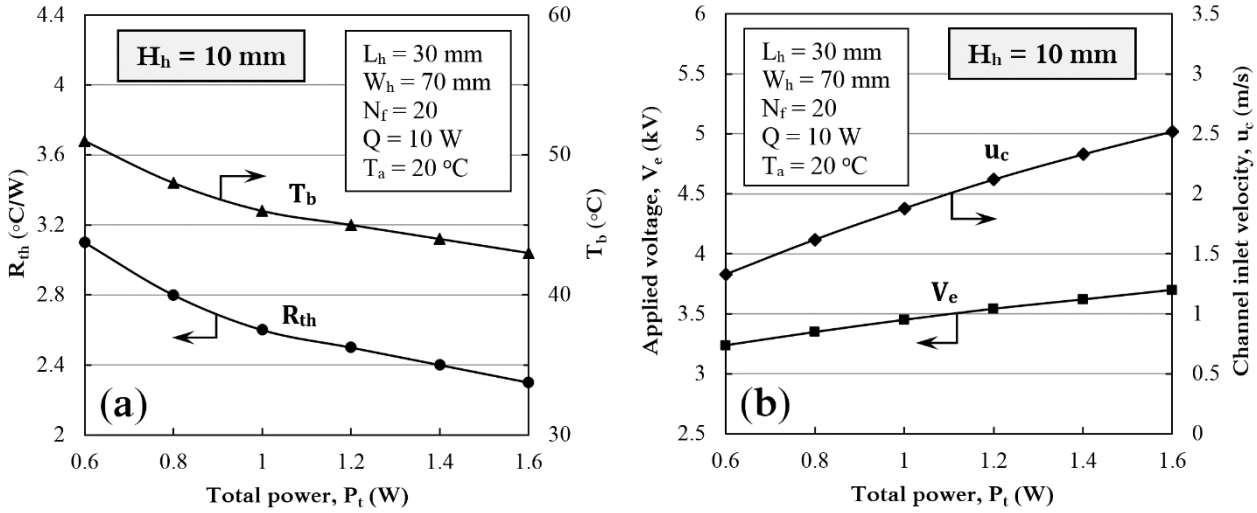

Fig. 13. Effect of operating power on (a) thermal resistance and base temperature, and (b) applied voltage and channel inlet velocity, for an EHD cooling system of H_h= 10 mm.

For example, the total operating power of the thinner cooling system (H_h= 6 mm) shown in **Fig. 12** can be increased from 0.6 to approximately 0.8 W at a fixed applied voltage of 3.5 kV by adding 7 fins and 6 wires. In this case, the drop in the temperature is expected to be higher compared to that shown in **Fig. 12**, (4 °C), using lower operating voltage. Indeed, achieving an appropriate balance between the levels of operating power and applied voltage, design of compact high-voltage multiplier, installation space of the cooling system and applied thermal power is essential in the practical implementation of EHD cooling systems in low height electronic devices.

5.5 Performance of EHD cooling system

The thermal performance of the developed EHD systems of different heights (6 – 12 mm) can be examined based on the applied thermal load or thermal design power (TDP), as it is usually called. The TDP is a good indicator that helps to determine the power efficiency and performance of a component, and is defined as the maximum amount of heat generated by a chip in the electronic device that the cooling system is designed to dissipate in typical operation [36]. All integrated EHD blowers are operated at a constant total power of 1.25 W, using (for this fixed power) different geometric and operating conditions, as listed in **Table 6**. The inlet air temperature is set at 30 °C, which is the expected value in real operations. The applied thermal load is varied from 10 to 30 W, and the heat dissipation capacity of each EHD cooling system is considered based on the highest temperature at the bottom surface of the heat sink base, T_b.

In this investigation, it is useful to use the maximum operating temperature allowed in laptops as a reference to evaluate the cooling performance of EHD systems proposed to be used in the same application field. NVIDIA states that the typical temperature of GPU, which is one of the hottest

running components in a computer, averages between 40 and 90 °C, with a maximum permissible operating GPU temperature of 105 °C before overheating [37]. In the present evaluation, the maximum temperature is assumed to be lower, namely 100 °C.

Fig. 14 shows the maximum temperature as a function of the thermal load for different heights of EHD systems, which are related to the geometric dimensions and operating conditions presented in **Table 6**. At a given total power of 1.25 W, the trends **A** and **B** reveal that thinner EHD cooling systems with heights of 6 and 8 mm are able to maintain the highest temperatures within the typical safe operating range under thermal loads up to 20 and 25 W, respectively, before they hit the region close to the maximum permissible temperature. When the EHD cooling systems become thicker (H_{h} = 10 and 12 mm), the trends **C** and **D** show improved cooling performance with keeping the highest temperatures within the safe range under a thermal load of 30 W.

Table 6 also shows that the error in the thermal resistance of the present modelling decreases compared to that calculated from equation (18) as the heat sink height increases, confirming that the accuracy of the analytical approach presented in [34] increases as the aspect ratio ($S_{\mathrm{f}}/H_{\mathrm{f}}$) decreases. It is useful to mention that further improvements can be achieved with lower operating temperatures by increasing the heat exchange area, which can be obtained by extending the width and length of the heat sink, or increasing the operating power per wire, which results in greater induced air velocities, depending on the requirements and limitations of the application itself.

In order to assess the capability of the present EHD cooling systems in real applications, a list of examples of the current standard laptops powered by Intel technology are selected and presented in **Table 7** as a guide for comparison, showing the max TDP and total thickness of different laptops. The figures reveal that the developed EHD cooling systems have great potential to compete with mechanical rotary fans in low-profile laptops with higher TDP and lower device height, even if the laptop screen thickness is added. Indeed, the ability of extending the width of the heat exchanger cooled by traditional centrifugal fans used in laptops is limited by the width of the fan exit region, which is always smaller than the total fan diameter. Furthermore, compared to conventional centrifugal fans, the present EHD system requires smaller installation volume even if the size of the compact high-voltage multiplier is included [7]. These significant advantages establish the integrated EHD cooling systems as a promising alternative thermal solution in low-profile laptop applications.

Table 6. Geometric dimensions and operating conditions used to examine the performance of developed EHD cooling systems.

Trend	H_h (mm)	L_h (mm)	W_h (mm)	N_f	A_{base} (mm^2)	P_w (W)	V_e (kV)	R_{th} (°C/W)	R_{th} [Eq. (18)] (°C/W)
A	**6**	30	124	35	3720	0.037	3.57	2.8	2.34
B	**8**	30	106	30	3180	0.043	3.47	2.3	2.00
C	**10**	30	88	25	2640	0.052	3.44	2.1	1.90
D	**12**	30	88	25	2640	0.052	3.35	1.8	1.65

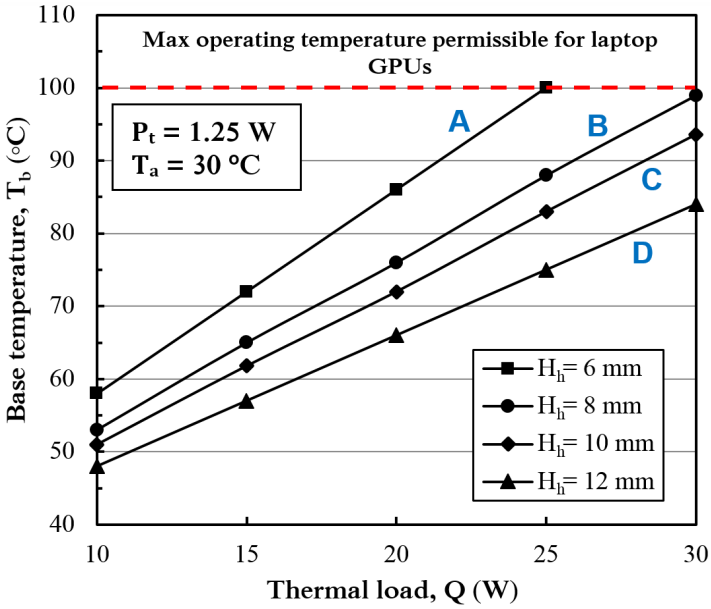

Fig. 14. Comparison of cooling performance of different EHD cooling systems, showing the base temperature as a function of the thermal load. Trends symbols are related to the information presented in **Table 6**.

Table 7. Examples of the current standard laptops powered by Intel technology available commercially [38].

Product	Max TDP	Total height
ASUS VivoBook S200E-CT320H notebook	17 W	20.9 mm
Acer Aspire 430	17 W	25.3 mm
Dell Latitude 7380 2.8GHz i7-7600U-13.3"	15 W	17.3 mm
ASUS VivoBook S510UA-BQ079T 2.4GHz i3-7100U-15.6"	15 W	17.9 mm
Lenovo IdeaPad 310-15 2GHz i3-6006U-15.6"	15 W	22.9 mm
Dell Latitude 3480 2.5GHz i5-7200U-14"	15 W	23.3 mm
ASUS Chromebook C300MA	7.5 W	20.3 mm
ASUS X553MA, 4Gb RAM, 750Gb Hard Drive, Wi-Fi, 15.6"	7.5 W	25.3 mm
Acer Aspire A114-31-C6S1 1.1GHz N3350 14"	6 W	18.0 mm
Lenovo N22 Chrome book - Celeron N3060 - 32GB Flash-11.6"	6 W	21.8 mm
ASUS VivoBook E201NA-GJ008T-OSS 1.1GHz N3350-11.6"	6 W	22.5 mm
ASUS VivoBook Max X541NA-GO230T 1.10GHz N4200 15.6"	6 W	27.6 mm
ASUS Zenbook UX305FA-FC004P 0.8GHz M-5Y10-13.3"	4.5 W	12.3 mm
HP EliteBook Folio 1020 G1 1.1GHz M-5Y51-12.5"	4.5 W	15.7 mm

6. Conclusions

The benefits of integrating EHD air blowers within parallel-plate heat sinks are investigated. A novel EHD cooling system is proposed as an effective thermal management solution for microelectronics and low-profile laptop applications. A three-dimensional numerical model is validated and developed to solve the coupled physics of EHD flow and conjugate heat transfer. For a range of heat sink heights from 6 to 12 mm, a parametric study is performed to investigate the effect of design parameters and operation conditions and evaluate the heat transfer characteristics and cooling performance of integrated EHD systems. Based on the results of the parametric study, the following conclusions can be drawn:

(1) The main dimensions of the heat sink (length, width and height) show significant effects on the dissipated and operating powers, and a delicate balance between these factors must be achieved for efficient design of EHD cooling systems.

(2) Unlike conventional rotary blowers, integrated EHD systems have a flexible design with the ability of reducing the height and increasing the width as required, offering a unique feature to be installed in low-profile laptops.

(3) At a given operating power of 1.25 W, predictions reveal that a compact EHD cooling system of 6 mm thickness, 124 mm width and 30 mm length, is able to maintain the operating temperature within the typical range, between 40 and 90 ^{o}C, under a thermal load (TDP) up to 20 W. By increasing the thickness to 12 and decreasing the width to 88 mm, the EHD system can maintain the operating temperature below 85 ^{o}C for a TDP of 30 W.

(4) Compared to traditional cooling systems used in the current standard laptops, the proposed EHD systems show promising cooling performance for laptops operating at higher TDP with reduced package volume and device thickness.

Acknowledgements

The 3D modelling work was undertaken on POLARIS, part of the High Performance Computing facilities at the University of Leeds, UK. Funding support from the Higher Committee for Education Development in Iraq (HCED Ref. No. D-11-3102) is gratefully acknowledged.

References

1. Wang, H.-C., N.E. Jewell-Larsen, and A.V. Mamishev, *Thermal management of microelectronics with electrostatic fluid accelerators.* Applied Thermal Engineering, 2013. **51**(1): p. 190-211.
2. Walsh, P., V. Egan, R. Grimes, and E. Walsh. *Scaling of Flow Characteristics and Power Consumption With Profile Height for Miniature Centrifugal Fans*. in *ASME 2007 5th International Conference on Nanochannels, Microchannels, and Minichannels*. 2007. American Society of Mechanical Engineers.

3. Day, S.W., P.P. Lemire, R.D. Flack, and J.C. McDaniel. *Effect of Reynolds Number on Performance of a Small Centrifugal Pump*. in *ASME/JSME 2003 4th Joint Fluids Summer Engineering Conference*. 2003. American Society of Mechanical Engineers.

4. Grimes, R., P. Walsh, E. Walsh, and V. Egan. *The Effects of Diameter and Rotational Speed on the Aerodynamic Performance of Low Profile Miniature Radial Flow Fans*. in *ASME 2007 5th International Conference on Nanochannels, Microchannels, and Minichannels*. 2007. American Society of Mechanical Engineers.

5. Egan, V., J. Stafford, P. Walsh, and E. Walsh, *An experimental study on the design of miniature heat sinks for forced convection air cooling.* Journal of Heat Transfer, 2009. **131**(7): p. 071402.

6. Fylladitakis, E.D., M.P. Theodoridis, and A.X. Moronis, *Review on the history, research, and applications of electrohydrodynamics.* Plasma Science, IEEE Transactions on, 2014. **42**(2): p. 358-375.

7. Jewell-Larsen, N., H. Ran, Y. Zhang, M. Schwiebert, K.H. Tessera, and A. Mamishev. *Electrohydrodynamic (EHD) cooled laptop*. in *Semiconductor Thermal Measurement and Management Symposium, 2009. SEMI-THERM 2009. 25th Annual IEEE*. 2009. IEEE.

8. Rickard, M., D. Dunn-Rankin, F. Weinberg, and F. Carleton, *Maximizing ion-driven gas flows.* Journal of Electrostatics, 2006. **64**(6): p. 368-376.

9. Moreau, E. and G. Touchard, *Enhancing the mechanical efficiency of electric wind in corona discharges.* Journal of Electrostatics, 2008. **66**(1): p. 39-44.

10. Colas, D.F., A. Ferret, D.Z. Pai, D.A. Lacoste, and C.O. Laux, *Ionic wind generation by a wire-cylinder-plate corona discharge in air at atmospheric pressure.* Journal of applied physics, 2010. **108**(10): p. 103306.

11. June, M.S., J. Kribs, and K.M. Lyons, *Measuring efficiency of positive and negative ionic wind devices for comparison to fans and blowers.* Journal of Electrostatics, 2011. **69**(4): p. 345-350.

12. Franke, M. and L. Hogue, *Electrostatic cooling of a horizontal cylinder.* Journal of heat transfer, 1991. **113**(3): p. 544-548.

13. Owsenek, B. and J. Seyed-Yagoobi, *Theoretical and experimental study of electrohydrodynamic heat transfer enhancement through wire-plate corona discharge.* Journal of Heat Transfer, 1997. **119**(3): p. 604-610.

14. Yonggang, Y., H. Junping, A. Zhongliang, Y. Lanjun, and Z. Qiaogen, *Experimental studies of the enhanced heat transfer from a heating vertical flat plate by ionic wind.* Plasma Science and Technology, 2006. **8**(6): p. 697.

15. Velkoff, H. and R. Godfrey, *Low-velocity heat transfer to a flat plate in the presence of a corona discharge in air.* Journal of Heat Transfer, 1979. **101**(1): p. 157-163.

16. Takimoto, A., Y. Tada, Y. Hayashi, and K. Yamada, *Convective heat-transfer enhancement by a corona discharge.* Heat Transfer-Japanese Research;(United States), 1991. **20**(1).

17. Shooshtari, A., M. Ohadi, and F.H. França. *Experimental and numerical analysis of electrohydrodynamic enhancement of heat transfer in air laminar channel flow*. in *Semiconductor Thermal Measurement and Management Symposium, 2003. Ninteenth Annual IEEE*. 2003. IEEE.

18. Go, D.B., R.A. Maturana, T.S. Fisher, and S.V. Garimella, *Enhancement of external forced convection by ionic wind.* International Journal of Heat and Mass Transfer, 2008. **51**(25): p. 6047-6053.

19. Go, D.B., S.V. Garimella, T.S. Fisher, and R.K. Mongia, *Ionic winds for locally enhanced cooling.* Journal of Applied Physics, 2007. **102**(5): p. 053302.

20. Go, D.B., R. Maturana, R.K. Mongia, S.V. Garimella, and T.S. Fisher. *Ionic Winds for Enhanced Cooling in Portable Platforms*. in *Electronics Packaging Technology Conference, 2008. EPTC 2008. 10th*. 2008. IEEE.

21. Hsu, C.-P., N.E. Jewell-Larsen, I.A. Krichtafovitch, and A.V. Mamishev, *Heat-transfer-enhancement measurement for microfabricated electrostatic fluid accelerators.* Journal of Microelectromechanical Systems, 2009. **18**(1): p. 111-118.

22. Schlitz, D. and V. Singhal. *An electro-aerodynamic solid-state fan and cooling system*. in *Semiconductor Thermal Measurement and Management Symposium, 2008. Semi-Therm 2008. Twenty-fourth Annual IEEE*. 2008. IEEE.

23. Huang, R.-T., W.-J. Sheu, and C.-C. Wang, *Heat transfer enhancement by needle-arrayed electrodes–An EHD integrated cooling system.* energy Conversion and Management, 2009. **50**(7): p. 1789-1796.

24. Shin, D.H., S.H. Baek, and H.S. Ko, *Development of heat sink with ionic wind for LED cooling.* International Journal of Heat and Mass Transfer, 2016. **93**: p. 516-528.

25. Karpov, S. and I. Krichtafovitch. *Electrohydrodynamic flow modeling using FEMLAB*. in *Excerpt from the Proceedings of the COMSOL Multiphysics User's Conference 2005 Boston*. 2005.

26. Feng, J.Q., *Application of Galerkin finite-element method with Newton iterations in computing steady-state solutions of unipolar charge currents in corona devices.* Journal of Computational Physics, 1999. **151**(2): p. 969-989.
27. Jewell-Larsen, N.E., G.G. Joseph, and K.A. Honer. *Scaling laws for electrohydrodynamic air movers*. in *ASME/JSME 2011 8th Thermal Engineering Joint Conference*. 2011. American Society of Mechanical Engineers.
28. Ramadhan, A.A., N. Kapur, J.L. Summers, and H.M. Thompson, *Numerical Analysis and Optimization of Miniature Electrohydrodynamic Air Blowers.* IEEE TRANSACTIONS ON PLASMA SCIENCE, 2017. **45**(11): p. 3007.
29. Kaptsov, N., *Elektricheskie yavleniya v gazakh i vakuume.* Moscow, OGIZ, 1947.
30. Peek, F.W., *Dielectric phenomena in high voltage engineering*. 1920: McGraw-Hill Book Company, Incorporated.
31. Jewell-Larsen, N.E., S.V. Karpov, I.A. Krichtafovitch, V. Jayanty, C.-P. Hsu, and A.V. Mamishev. *Modeling of corona-induced electrohydrodynamic flow with COMSOL multiphysics*. in *Proc. ESA Annual Meeting on Electrostatics, Paper E*. 2008.
32. Ramadhan, A., N. Kapur, J. Summers, and H. Thompson, *Numerical modelling of electrohydrodynamic airflow induced in a wire-to-grid channel.* Journal of Electrostatics, 2017. **87**: p. 123-139.
33. Kim, S.J., D.-K. Kim, and H.H. Oh, *Comparison of fluid flow and thermal characteristics of plate-fin and pin-fin heat sinks subject to a parallel flow.* Heat Transfer Engineering, 2008. **29**(2): p. 169-177.
34. Teertstra, P., M. Yovanovich, and J. Culham, *Analytical forced convection modeling of plate fin heat sinks.* Journal of Electronics Manufacturing, 2000. **10**(04): p. 253-261.
35. LPTPS.com. *Best laptops Guides & Reviews*. 2017; Available from: http://www.lptps.com/best-ultra-thin-laptops/.
36. Do, T., S. Rawshdeh, and W. Shi, *ptop: A process-level power profiling tool*, 2009, HotPower.
37. NVIDIA. NVIDIA SUPPORT; Available from: http://www.nvidia.co.uk/object/support-uk.html.
38. Intel. Standard Laptops Powered by Intel Technology, October 2017; Available from: https://www.intel.co.uk/content/www/uk/en/products/devices-systems/laptops/standard.html.